Mango Kernel-Derived Porous Carbon Confines Nano-NiO as an Efficient Bifunctional Electrode for Supercapacitors

Bing Wang,[a,c] Suping Li,[a] Liansheng Cui,[a] Shuai Wang,[c] Xuan Zhang,[c] Yonggang Li, [a,*] and Ziao Zong,[b,*]

In order to develop high-performance supercapacitor electrode materials, a two-step method of hydrothermal *in-situ* synthesis and high-temperature activated pore creation was used to realize the highly dispersed loading of nickel oxide nanoparticles (NiO) on mango kernel-based activated carbon (AC) with a high specific surface area for the preparation of NiO/AC composites. Electrochemical tests showed that the NiO/AC achieved a specific capacitance of 226.5 F g^{-1} at a current density of 0.2 A g^{-1}, demonstrating excellent multiplicative performance and cycling stability (95.8% capacitance retention after 10,000 charge/discharge cycles). This performance stems from the stabilized multilayered pore structure that reduces the particle size of NiO and builds fast ion/electron transport channels to realize the dual advantages of double layer capacitance and pseudocapacitance. The present synthesis strategy is universal (compatible with multifunctional porous carbon precursors and metal oxides) and can provide new ideas for the design of high-performance supercapacitor electrodes.

DOI: 10.15376/biores.20.4.11056-11065

Keywords: Ultracapacitor; Raw materials; Hydrothermal; Nickel oxide; Capacitor performance

*Contact information: a: Guangxi Key Laboratory of Urban Water Environment, College of Chemistry and Environmental Engineering, Baise University, Baise 533000, China; b: Modern Industrial College of Biomedicine and Great Health, Youjiang Medical University for Nationalities, Baise533000, China; c: School of Environment and Resources, Taiyuan University of Science and Technology, 66 Wa-liu Road, Taiyuan,030024, Shanxi, China; *Corresponding authors: li.yonggang@126.com; zongziao@126.com*

INTRODUCTION

With the continuous growth of global energy demand and the over-consumption of traditional fossil energy sources, the problems of energy shortage and environmental pollution are becoming more and more serious, driving the urgent need for clean and efficient energy storage technologies. As a new type of energy storage device with high power density, fast charging and discharging capability and long cycle life, supercapacitors have shown broad application prospects in new energy vehicles, smart grids and portable electronic devices such as smartphones, wearable health monitoring devices, and portable unmanned aerial vehicle power supplies (Yaday and Tripathi 2017). The core of supercapacitor performance depends on the design and preparation of electrode materials. Widely researched electrode materials include carbon-based materials, metal oxides, and conductive polymers (Li *et al.* 2016). Carbon-based materials have become a typical representative of bilayer capacitors by virtue of their good chemical stability, rich pore structure, and low-cost advantages, but their energy density is limited by the purely

physical storage mechanism, and the specific capacitance is relatively low (Sonadia *et al.* 2025). Metal oxides (*e.g.*, NiO), on the other hand, provide pseudo-capacitance through reversible redox reactions and have a significantly higher theoretical specific capacitance than carbon materials (Zhang *et al.* 2014), however, their poor electronic conductivity and significant volume expansion lead to suboptimal cycle life (Nagaraju *et al.* 2022).

The composite of carbon-based materials and metal oxides to construct new electrodes can realize the synergistic effect of double-layer capacitance and pseudo-capacitance, which becomes an important strategy to enhance the performance of supercapacitors (Yin and Park 2015). Although some studies have enhanced the specific capacitance performance through the multicomponent synergistic effect of composites, the multiplicity performance and cycling stability are still subject to multiple constraints. First, the electrode material triggers lattice stress accumulation due to ion embedding and dislodging during repeated charging and discharging, and the difference in elastic modulus between the active substance and the conductive carrier leads to microcracks at the interface, resulting in fracture of the conductive network and deterioration of the charge transport path (Priyadharshini *et al*. 2025). Second, heterogeneous interfaces form dynamic barriers due to lattice distortions during cycling, which impede electron/ion transport across the interface, leading to a decline in the kinetic properties (Choi *et al*. 2017).

In this work, activated carbon (AC) having a hierarchical pore structure was prepared using an carbonization and activation etching processes using mango kernel, a characteristic waste biomass in Guangxi region of China, as a green carbon source. The *in situ* hydrothermal synthesis method was further employed to grow NiO nanoparticles in the restricted domain inside the pores to construct the AC/NiO gradientized composite electrode materials. This innovative structural design fully utilizes the spatial confinement effect of porous carbon and effectively inhibits the agglomeration of NiO nanoparticles. Meanwhile, the three-dimensional interconnected conductive carbon skeleton is complemented with natural nitrogen doping modification, which not only builds an efficient channel for ion transport, but it also shortens the ion transport path. As verified by electrochemical tests, the composite electrode material exhibits high specific capacity, excellent multiplicity performance and cycling stability, which provides a new idea and direction for the development of electrode materials for high-performance supercapacitors.

EXPERIMENTAL

Materials

All chemicals (analytical reagent) used to perform the experiments were purchased from Aladdin Reagents (Shanghai) Co., Ltd. and used without further purification. All solutions used during the experiments were prepared with deionized water.

Preparation of mango kernel based activated carbon

Cleaned mango kernels (MB) were crushed to less than 100 mesh and dried to constant weight. A total of 10 g of mango kernel powder was taken and heated to 400 °C at 5 °C min $^{-1}$ under nitrogen protection and kept for 2 h. The carbonized material was obtained after cooling. The carbonized material was mixed with KOH solution (concentration 10 mol L^{-1}) at a mass ratio of 2:1 in a porcelain boat and impregnated at a constant temperature of 80 °C for 12 h. The ceramic boat was then heated to 800 °C at 5 °C min $^{-1}$ under nitrogen protection, and the mixture was held for 3 h. The cooled product

was washed to neutrality with deionized water and dried to produce mango kernel-based activated carbon, named MBAC.

Nano NiO preparation

After dissolving 0.2377 g of $NiCl_2 \cdot 6H_2O$ in 50 mL of deionized water, 1 mL of a 1 M urea solution was added. After stirring for 30 min, the mixed solution was poured into a 100 mL reaction kettle and reacted for 6 h in an oven at 110 °C. The reacted solution was cooled to room temperature, centrifuged, washed several times with deionized water and anhydrous ethanol, and dried. The final powder sample NiO was calcined at 400 °C for 3 h.

MBAC/NiO preparation

After dissolving 0.2377 g of $NiCl_2 \cdot 6H_2O$ in 50 mL of deionized water, 2 g of AC was added; 1 mL of 1 M urea solution was added after stirring for 30 min. The mixed solution was poured into a 100 mL reaction kettle and reacted for 6 h in an oven at 110 °C. The reacted solution was cooled to room temperature, centrifuged, washed several times with deionized water and anhydrous ethanol, dried, and named MBAC/$Ni(OH)_2$. Finally, the final powder sample MBAC/NiO was obtained by calcination at 400 °C for 3 h.

Preparation of electrode materials

The three materials, MBAC, NiO, and MBAC/NiO, were mixed with carbon black and PVDF (heated and dissolved in an appropriate amount of NMP) in the ratio of 8:2.5:1 by mass to form a slurry. The slurry was uniformly applied on 15 mm×10 mm nickel foam and weighed after drying in a vacuum oven at 80 °C for 2 h. The mass of the active substance of the working electrode was calculated. The active material loading range for single electrodes is 1.0 to 1.5 mg cm^{-2}.

Characterization and Testing

The microstructure of the samples was analyzed using scanning electron microscopy (SEM, ZEISS EVO18, Germany) and transmission electron microscopy (TEM, ZEISS Sigma 500, Germany) techniques. The X-ray photoelectron spectroscopy (XPS, PE PHI-1600, America) technique was used to analyze the surface chemical properties of the samples. The electrochemical performance of electrodes was tested by electrochemical workstation (CHI600E, Shanghaichenhua), and a solution of Na_2SO_4 (1 M) was used as the electrolyte. A three-electrode system, consisting of working (MBAC, NiO and MBAC/NiO), reference (saturated calomel electrode), and counter (platinum plate electrode of dimensions 15 mm ×10 mm) electrodes, was used for electrodes analysis.

The charge–discharge curves were analyzed, and the specific capacitance of the electrodes was obtained using Eq. (1) as follows,

$$C = \frac{I \times \Delta t}{m \times \Delta U} \quad (1)$$

where I (A), Δt (s), and ΔU (V) represent the discharge current, time, and potential interval after deducting the ohmic drop, respectively. In the three-electrode system, m(g) represents the mass of the active material in a single electrode and both electrodes, respectively.

RESULTS AND DISCUSSION

Morphology Analysis

Scanning electron microscopy (SEM) images showed (Fig. 1a) that MBAC exhibited a typical lumpy and flaky interwoven morphology, which is a common structural feature of conventional activated carbon. Its surface was distributed with different sizes of slit pores, but the regularity and uniformity of the pore structure was poor. The macropores and mesopores of activated carbon mainly assume the role of electrolyte transport channels, while the inner surfaces of micropores and mesopores are the main contributing regions to the capacitance of the double layer (Liu *et al*. 2015). However, irregularities in the distribution of the pores may affect the full contact of the electrolyte with the inner surface, which in turn limits the full performance of its capacitance.

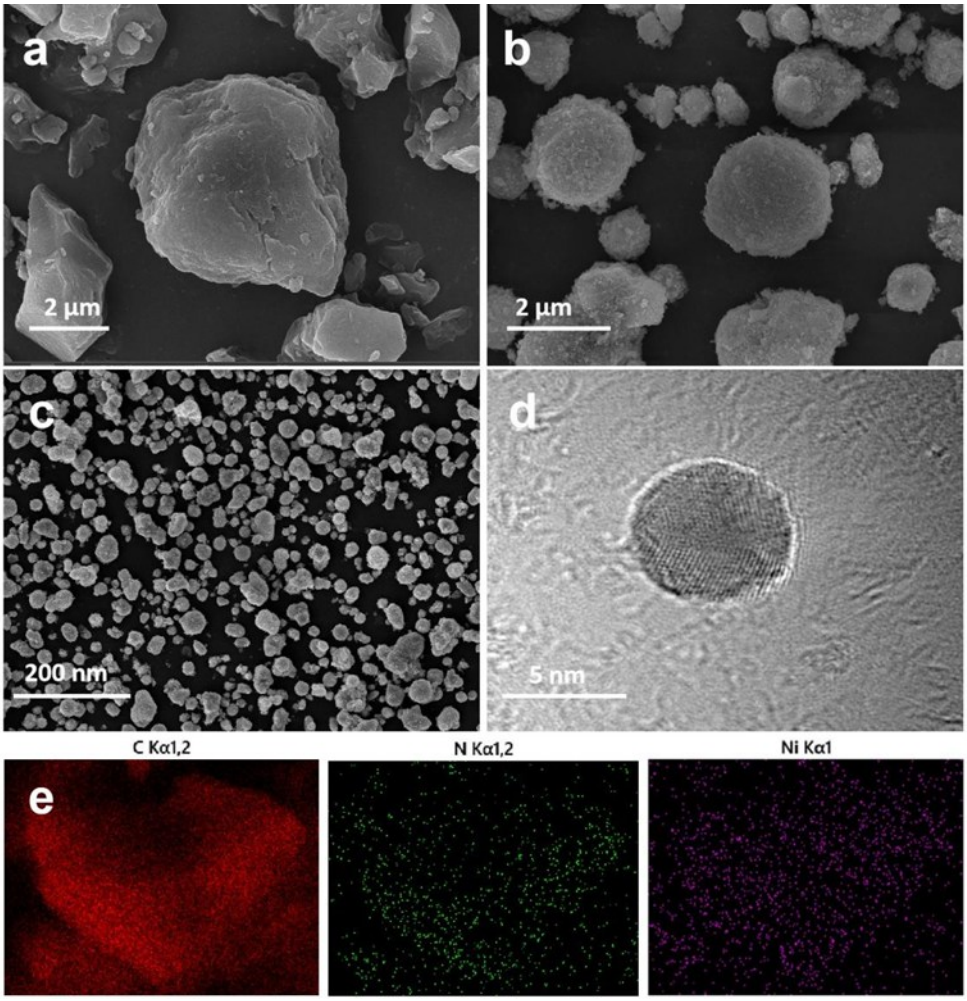

Fig. 1. Scanning electron microscopy (SEM) images recorded for (a) MBAC, (b) NiO, and (c) MBAC/NiO. (d) Transmission electron microscopy (TEM) images and (e) element mapping profiles corresponding to C, N, and Ni in MBAC/NiO

Figure 1b shows that the NiO particles were large, with obvious agglomeration. This may be related to the growth kinetics of NiO crystals under hydrothermal reaction conditions (To *et al*. 2014). Although agglomeration is difficult to avoid in the preparation of nanomaterials, excessive agglomeration reduces the specific surface area of the material,

which in turn affects its exposure to electrochemical active sites as pseudocapacitive actives (Malik *et al*. 2024). Therefore, controlling the degree of agglomeration of NiO is essential to optimize its electrochemical performance. At the 200 nm scale (Fig. 1c-d), the hierarchical porous structure of MBAC constructed a hierarchical spatial confinement system. The diameter of micropores matched the NiO precursor ions, serving as nanoreactors. Mesopores act as "ion transport channels" to reduce diffusion resistance, while macropores accommodate the volume expansion of NiO during charge-discharge cycles. This multi-scale confinement synergistically inhibits NiO agglomeration, and its highly dispersed nanomorphology facilitates the construction of a synergistic effect between the double layer capacitance and the pseudocapacitance (Fayed *et al.* 2025). Transmission electron microscopy (TEM) with elemental mapping analysis (Fig. 1e) confirmed that nickel oxide clusters were uniformly distributed on the surface of the activated carbon matrix. In addition, a small amount of nitrogen distribution was observed, and this doping may be attributed to the natural nitrogen component of mango kernels and the introduction of nitrogen-containing reactants (urea) during the preparation process (Zhao *et al*. 2016). Nitrogen atoms (with higher electronegativity than carbon) doped into carbon materials form different functional groups such as pyridine nitrogen, pyrrole nitrogen, graphite nitrogen, *etc*. These nitrogen sites provide additional pseudocapacitance through redox reactions and improve multiplicity performance (Li *et al*. 2024).

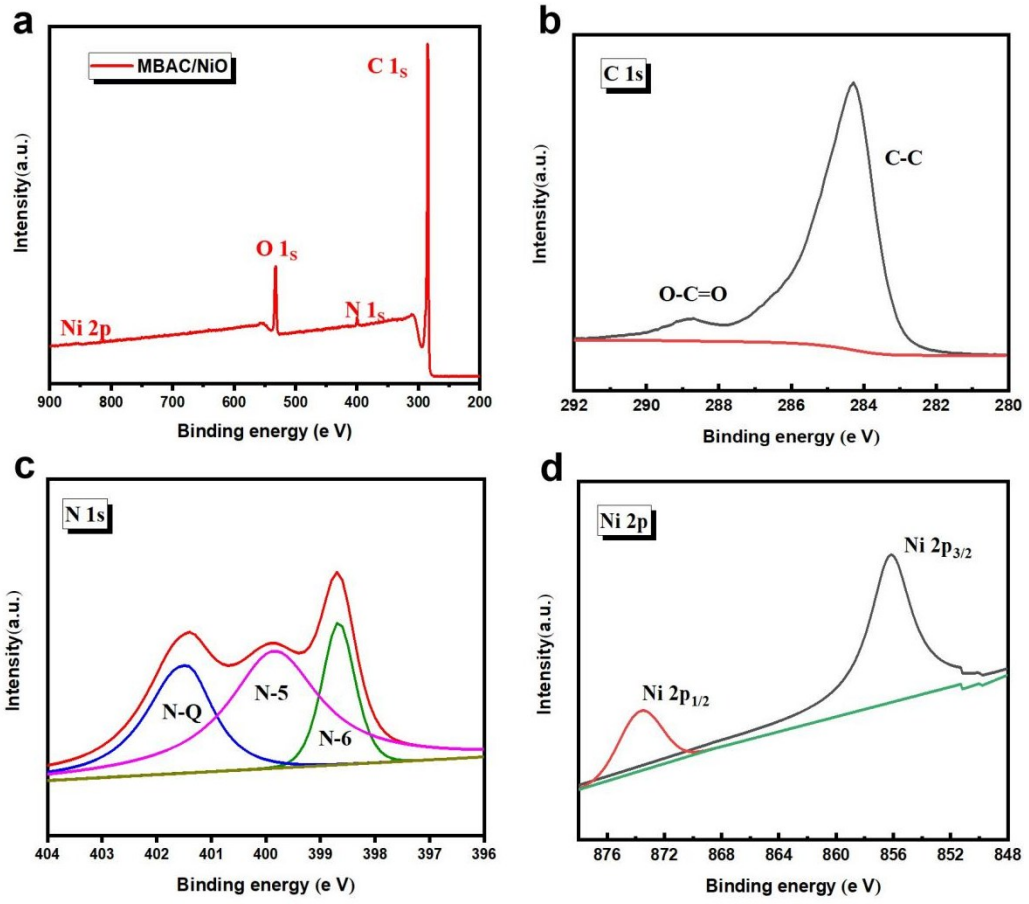

Fig. 2. XPS survey of MBAC/NiO (**a**), Deconvolution curves of C1s (**b**), N1s (**c**) and Ni2p (d)

Structure Analysis

Three peaks at 285 eV, 400 eV, and 533 eV, corresponding to the C1s, N1s, and O1s peaks, respectively, were observed in the wide-scan XPS spectra of MBAC/NiO (Fig. 2a), but the Ni2p peaks were not obvious. The C1s peaks were fitted and analyzed (Fig. 2b), and the two main characteristic peaks located at 284.3 and 288.8 eV correspond to C-C and O-C=O, respectively. Oxygen atoms participate in the Faraday reaction in the form of carbonyl groups; these groups improve the surface wettability of carbon materials (Chute *et al*. 2024). The N1s peaks were fitted and analyzed (Fig. 2c), and the three major peaks represented pyridine N (N-6 at 398.6 eV, 31.2%), pyrrole N (N-5 at 399.8 eV, 41.5%), and quaternary N (N-Q at 401.5 eV, 27.3%). N-5 exhibited good electron-donor properties and high charge mobility, which helped to enhance the catalytic activity in electron transfer reactions; N-6 can provide a pair of electrons to conjugate with the π-conjugated ring, which is crucial for the contribution to the pseudocapacitance, and N-Q contributes to the increase of the electrical conductivity of carbon materials (Zhang *et al*. 2016). The Ni2p peak (Fig. 2d) was fitted as two peaks with binding energies of 856.1 eV and 873.8 eV, which correspond to the $2p_{1/2}$ and $2p_{3/2}$ orbitals of Ni in nickel oxide, and its energy level properties can synergistically enhance the capacitive performance by influencing the electron transfer and ion adsorption (Yadav *et al*. 2024).

Electrochemical Performance of Supercapacitors

Figure 3a presents the cyclic voltammetry (CV) curves of MBAC, NiO and MBAC/NiO at a scan rate of 5 mV s^{-1}. The CV curves of MBAC exhibited a nearly rectangular profile without obvious redox peaks, reflecting the typical electric double layer capacitance (EDLC) behavior, which originates from the reversible adsorption/desorption process of the surface charge of carbon materials. The CV curves of NiO show redox peaks corresponding to the Faraday pseudocapacitive response of Ni^{2+}/Ni^{3+}, but the peak currents were low, reflecting the impeded charge transport due to its intrinsic poor conductivity (Pan and Dong 2024).

In contrast, the CV curve area of MBAC/NiO was significantly larger than that of either material alone. This composite material retains the electric double-layer capacitance contribution of MBAC while exhibiting the pseudocapacitance contribution of NiO ($NiO + OH^- \leftrightarrow NiOOH + e^-$). This synergistic effect stems from the hierarchical porous structure and highly conductive network constructed by MBAC, which effectively reduces the particle size and charge transport resistance of NiO and promotes the kinetic process of the pseudocapacitive reaction, thus enhancing the overall capacitance density (Liu *et al*. 2024).

Figure 3b shows the constant current charge/discharge curve at 0.2 A g^{-1} current density, with symmetry reflecting reaction reversibility. The curve of MBAC is close to a symmetric rectangle with a short discharge time, corresponding to a lower specific capacitance (determined by the EDLC mechanism). There is a significant tilt in the curve of NiO with short discharge time and poor symmetry, indicating a significant polarization effect and limited reversibility of the pseudocapacitive reaction (Vinodh *et al*. 2022). The curve of MBAC/NiO was closer to the symmetric triangle and had the longest discharge time. The calculated specific capacitance of MBAC/NiO at 0.2 A g^{-1} was 226.5 F g^{-1}, which was significantly higher than MBAC (143.8 F g^{-1}) and NiO (193.9 F g^{-1}). This stems from the fact that the introduction of MBAC enhanced the reversibility of the NiO pseudocapacitance reaction, and the carbon skeleton accelerated electron/ion transport and suppresses polarization. Figure 3c examines the variation rule of specific capacitance with current density, and all three specific capacitances decreased with increasing current

density. This is attributed to ion diffusion lag at high currents and reduced active site utilization. NiO showed the fastest specific capacitance decay, stemming from high polarization due to insulating properties and impeded charge transport at high currents. MBAC had a slow specific capacitance decay but low base capacity, reflecting the rate advantage of EDLC but insufficient capacity. MBAC/NiO exhibited the highest specific capacitance (153 153 F g^{-1} at 2.0 A g^{-1}) across the full range of current densities, realizing a "high capacity - high speed" balance: the conductive network of the MBAC guarantees electron migration at high currents. NiO's pseudocapacitance provides high capacity, and interfacial interaction promotes ion diffusion, synergistically enhancing the rate performance (Li *et al*. 2018). MBAC/NiO was retained at 95.8% after 10,000 cycles at 2 A g^{-1} (Fig. 3d), which resulted from the dual role of the MBAC porous carbon skeleton. Unlike traditional physically mixed NiO/AC composites, MBAC effectively inhibited the volume expansion of NiO during charge-discharge processes through the in-situ synthesis of NiO. This chemically coupled interface simultaneously enhances electrical conductivity and structural stability (Zhang *et al*. 2014).

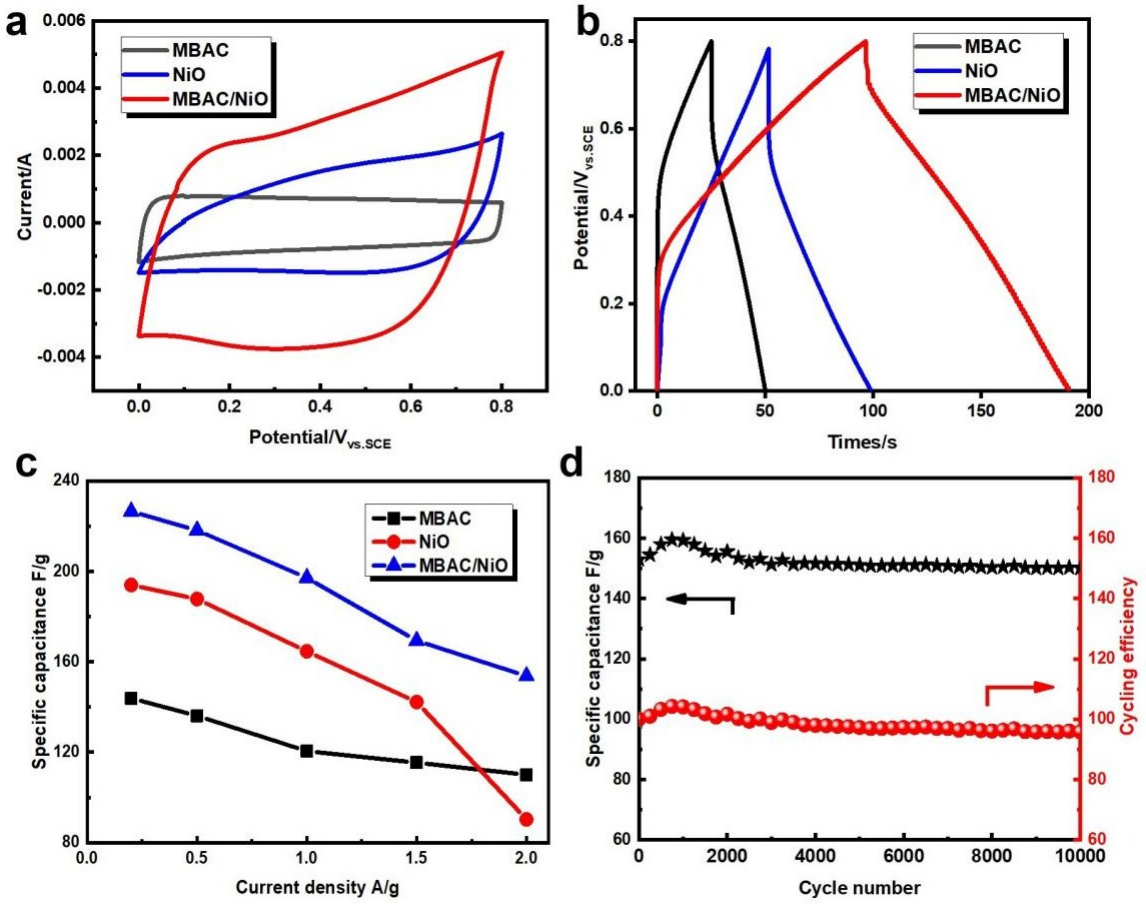

Fig. 3. Electrochemical performance of MBAC, NiO, and MBAC/NiO, studied using a three-electrode system: (a) Cyclic voltammetry recorded at 5 mV s^{-1}. (b) Galvanostatic charge–discharge curves recorded at 0.2A g^{-1}. (c) Specific capacitance recorded under conditions of varying current densities. (d) Cyclic stability recorded at a charge–discharge current density of 2A g^{-1} after 10 000 cycles for MBAC/NiO

CONCLUSIONS

1. A two-step method of hydrothermal *in situ* synthesis combined with high-temperature activation for pore creation was successfully used to achieve highly dispersive loading of NiO nanoparticles on the surface of mango kernel-based activated carbon (MBAC) with high specific surface area. This strategy utilized the multilayered pore structure of the carbon matrix to provide stable anchor sites for NiO nanoparticles to avoid agglomeration, and constructed a "conductive carbon skeleton-highly reactive oxide" composite interface.
2. MBAC/NiO exhibited a specific capacitance of 226.5 F · g^{-1} at a current density of 0.2 A g^{-1}, which is significantly higher than that of a single carbon material (double-layer capacitance) or pure NiO (low conductivity limitation), reflecting the synergistic gain of the double-layer capacitance and pseudocapacitance.
3. The capacitance retention reached 67.8% when the current density was increased from 0.2 to 2 A g^{-1}, which is attributed to the fast electron transport channel of the carbon matrix and the short ion diffusion path of the NiO nanoparticles. After 10,000 charge/discharge cycles, the capacitance loss was only 4.2%, verifying the effective buffering of the composite structure against the bulk effect (expansion and contraction in the NiO pseudocapacitance reaction). This simple synthesis method is expected to promote the practical application of high-performance supercapacitors in portable electronic devices and energy storage systems.

ACKNOWLEDGEMENTS

This work was financially supported by General Project of Guangxi Natural Science Foundation (2025GXNSFAA069295), Guangxi First-class Disciplines (Agricultural Resources and Environment)，Fundamental Research Program of Shanxi Province (202403021212115), Research Project Supported by Shanxi Scholarship Council of China (2024-124), Doctoral Research Initiation Fund of Taiyuan University of Science and Technology (N20242051), Taiyuan University of Science and Technology rewarded funds for excellent doctors working in Shanxi Province (No.20242124).

REFERENCES CITED

Chute, K. N., Mangate, N. V., Shiwankar, N. B., and Giripunje, S. M. (2024). "NiO impregnated peanut shell activated carbon (Ni/PSAC): Unveiling its redox potentiality for supercapacitor application," *Materials Letters* 361, article 136150. DOI: 10.1016/j.matlet.2024.136150

Fayed, M. G., Aman, D., and Mohamed, S. G. (2025). "Synergetic electrochemical behavior of NiO and activated carbon composites for advanced supercapacitors," *Journal of Cluster Science* 36, article 94. DOI: 10.1007/s10876-025-02804-3

Kahimbi, H., Hong, S. B., Yang, M. H., and Choi, B. G. (2017). "Simultaneous synthesis of NiO/reduced graphene oxide composites by ball milling using bulk Ni and graphite oxide for supercapacitor applications," *Journal of Electroanalytical Chemistry* 786, 14-19. DOI: 10.1016/j.jelechem.2017.01.013

Li, H., Mi, W., Zhang, F., Song, Y., and Zhao, J. (2024). "Microwave-assisted hydrothermal synthesis of NiO/Co_3O_4 nanosheets decorated on three-dimensional porous graphene for supercapacitors," *The Journal of Physics and Chemistry of Solids* 190, article 112025. DOI:10.1016/j.jpcs.2024.112025

Li, Q., Wei, Q., Xie, L., Chen, C. M., Lu, C., Su, F., and Zhou, P. (2016). "Layered NiO/reduced graphene oxide composites by heterogeneous assembly with enhanced performance as high-performance asymmetric supercapacitor cathode," *RSC Advances* 6, 46548-46557. DOI: 10.1039/C6RA04998B

Li, X., Liu, Y., Jin, Z., Li, P., Chen, X., and Xiao, D. (2018). "Enhanced electrochemical performance of C-NiO/$NiCo_2O_4$//AC asymmetric supercapacitor based on material design and device exploration," *Electrochimica Acta* 296, article 11. DOI: 10.1016/j.electacta.2018.11.011

Liu, G., Sun, Y.J., Guo, X., Yang, C., Cheng, Y., and Liu, D. (2024). "Improving charge transfer *via* nickel–nickel oxide/molybdenum dioxide heterostructure for advanced supercapacitor electrode," *Electrochimica Acta* 478, article 9. DOI: 10.1016/j.electacta.2024.143863

Liu, M., Chang, J., Bai, Y., and Sun, J. (2015). "An advanced asymmetric supercapacitor based on a novel ternary graphene/nickel/nickel oxide and porous carbon electrode with superior electrochemical performance," *RSC Advances* 5, 10.1039.C5RA18976D. DOI: 10.1039/C5RA18976D

Malik, R., Lekshmi, M. P. G., Rana, A., Rana, M., Srivastava, R., and Suman, C. K. (2024). "Study of synergistic nanostructures of NiO/ZnO and their composite as high-performance electrodes for supercapacitor," *Bulletin of Materials Science* 47(4), 1-9. DOI: 10.1007/s12034-024-03308-y

Nagaraju, Y. S., Ganesh, H., Veeresha, S., Vijeth, H., and Devendrappa, H. (2022). "Synthesis of hierarchical ZnO/NiO nanocomposite Wurtz hexagonal nanorods *via* hydrothermal for high-performance symmetric supercapacitor applications," *Journal of Energy Storage* 56(Part A), article 105924. DOI: 10.1016/j.est.2022.105924

Pan, C., and Dong, L. (2024). "Design and synthesis of $NiCo_2O_4$@Au@NiO sandwiched coaxial core–shell nanowire arrays on carbon fabric for high-performance supercapacitor," *Journal of Materials Science: Materials in Electronics* 35(8). DOI: 10.1007/s10854-024-12306-z

Priyadharshini, P., Vanasundari, K., Sureka, P., and Mahalakshmi, G. (2025). "Honeycomb-like open-edged reduced-graphene-oxide (rGO)-incorporated NiO/Co_3O_4 as advanced cathodes as hybrid supercapacitors for energy storage device applications," *Journal of Materials Science: Materials in Electronics* 36(11), 1-14. DOI: 10.1007/s10854-025-14734-x

Sonadia, M. W., Iqbal, Z., Shah, M., Mustafa, G., Mushtaq, M. U., Ul-Hamid, A., and Azad, F. (2025). "High-performance cauliflower-like Er_2O_3/NiO nanocomposite derived from Er-Ni-MOF for energy conversion and storage applications," *Journal of Energy Storage* 108, article 115222. DOI: 10.1016/j.est.2024.115222

To, A.C., Chen, D., Yang, X., and Du, Y. (2014). "Silver nanoparticles decorated on a three-dimensional graphene scaffold for electrochemical applications," *Journal of Physics and Chemistry of Solids* 75(1), 109-114. DOI: 10.1016/j.jpcs.2013.09.006

Vinodh, R., Babu, R.S., Atchudan, R., Kim, H.-J., Yi, M., Samyn, L., and de Barros, A.L.F. (2022). "Fabrication of high-performance asymmetric supercapacitor consists of nickel oxide and activated carbon (NiO//AC)," *Catalysts* 12(4), article 375. DOI: 10.3390/catal12040375

Yadav, D. D., Kumar, A., Jha, R., and Singh, S. (2024). "Flexible Fe-doped NiO/Ni-foam substrate nano-system based electrode with tunable opto-electrochemical attributes for supercapacitor applications," *Journal of the Electrochemical Society* 171(12). DOI: 10.1149/1945-7111/ad97e6

Yaday, S. T., and Tripathi, S. K. (2017). "Synthesis and characterization of nanocomposite NiO/activated charcoal electrodes for supercapacitor application," *Ionics* 23(10), 2919-2930. DOI: 10.1007/s11581-017-2026-9

Yin, J. L., and Park, J. Y. (2015). "Asymmetric supercapacitors based on the in situ-grown mesoporous nickel oxide and activated carbon," *Journal of Solid State Electrochemistry* 19(8), 2391-2398. DOI: 10.1007/s10008-015-2885-9

Zhang, L., Zheng, W., Jiu, H., Ni, C., and Qi, G. (2016). "The synthesis of NiO and $NiCo_2O_4$ nanosheets by a new method and their excellent capacitive performance for asymmetric supercapacitor," *Electrochimica Acta* 215, 212-222. DOI: 10.1016/j.electacta.2016.08.099

Zhang, Z., He, Y., Zhou, Q., Huang, C., Zhang, X., Guo, Z., Gao, Y., Liu, J., and Cao, Z. (2014). "Unique Ni@NiO core-shell/AC composite for supercapacitor electrodes," *Electrochimica Acta* 144(1), 300-306. DOI: 10.1016/j.electacta.2014.08.059

Zhao, J., Li, Z., Zhang, M., Meng, A., and Li, Q. (2016). "Direct growth of ultrathin $NiCo_2O_4$/NiO nanosheets on SiC nanowires as a free-standing advanced electrode for high-performance asymmetric supercapacitors," *ACS Sustainable Chemistry & Engineering* 4(7), 3598-3608. DOI: 10.1021/acssuschemeng.6b00697

Article submitted: July 2, 2025; Peer review completed: September 27, 2025; Revised version received: October 1, 2025; Accepted: October 25, 2025; Published: November 1, 2025.
DOI: 10.15376/biores.20.4.11056-11065